Organo-modified bentonite for gentamicin topical application: Interlayer structure and in vivo skin permeation

Valentina Iannuccelli, EleonoraMaretti, Alessia Bellini, Daniele Malferrari, Guido Ori, Monia Montorsi, Moreno Bondi, Eleonora Truzzi, Eliana Leo

Highlights

An organo-modified raw bentonite was developed as novel antibacterial material.

Thermal reactions could support drug intercalation occurrence.

MD simulations showed gentamicin monolayer arrangement within Mnt interlayer.

Trans-epidermal route was favored by drug intercalation as arisen from *in vivo* data.

Abstract

Recent biomedical applications of clay materials have included organically modified clays or clay minerals with the purpose of modifying and improving drug biological activity. The present research aims to explore the potential benefits provided by a raw bentonite (Bt) modified by gentamicin (GM) adsorbed within montmorillonite interlayers in the management of cutaneous infectious diseases. Information arisen from controlled X-ray powder diffraction, thermogravimetry coupled with evolved gas mass spectrometry, and molecular dynamics simulations pointed out GM monolayer arrangement within montmorillonite framework without producing substantial effects on the layer periodicity. Concerning skin biomedical application, unlike the pure antibiotic permeating along the trans-follicular pathway across *stratum corneum*, the organo-modified Bt/GM would favor the trans-epidermal route along inter-cluster corneocyte region, as *in vivo* skin penetration studies by means of tape stripping test indicated. Based on the results obtained, GM intercalation could represent a potential advantageous approach allowing a long-term Bt/GM reservoir for sustained antibacterial activity.

Graphical abstract

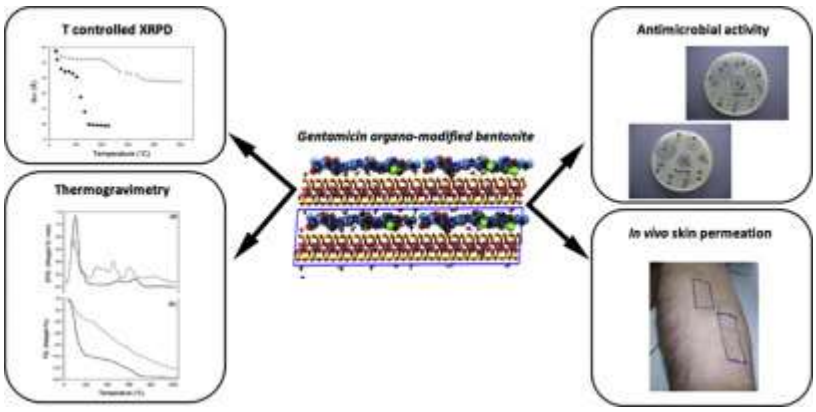

Keywords

Bentonite, Gentamicin, Intercalation, Thermal analyses, Molecular dynamics, *In vivo* skin penetration

1. Introduction

There is a strong demand to identify new strategies in order to set optimal drug delivery systems for antibiotic treatments. Intercalation of organic molecules into layered inorganic solids provides a useful and convenient approach to prepare hybrids that show properties of both the inorganic host and organic guest in a single material (Aguzzi et al., 2007; Rodrigues et al., 2013). In the last five decades the ability of both raw and synthetic smectites to exchange cations with several organic compounds has been exploited in many application fields. An archetypical example of such versatility is represented by the polymeric nanocomposites employing organo-modified bentonites (Benelli et al., 2017; Franchini et al., 2008; 2011; Morgan and Wilkie, 2007).

More recently, smectites have been proposed as materials for modulating drug delivery or improving dissolution of poorly water-soluble drugs (Aguzzi et al., 2005; Iannuccelli et al., 2015; Joshi et al., 2009). Among smectites, the 2:1 layered montmorillonite is probably the most investigated clay mineral. The reasons that drive this interest mainly arise from its high specific surface area, swelling and adsorptive capacity, high cation exchange capacity (CEC), specific rheological properties, drug-carrying capability and ability to modulate drug release (World Health Organization, 2005). Montmorillonite is mainly used as auxiliary material in the pharmaceutical industry for oral or topical dosage forms, recorded in the United States, European, and British Pharmacopeias. Montmorillonite, following to its high swelling behavior, can intercalate therapeutic compounds between the layers generating a host for oral or topical drug delivery (Aguzzi et al., 2005; Bello et al., 2015; Bonina et al., 2007, p. 200; de Paiva et al., 2008; Forni et al., 1987; Iannuccelli et al., 2015; Iliescu et al., 2011; Joshi et al., 2009; Kant and Datta, 2016; Katti et al., 2010; Kim et al., 2016; Mohamed et al., 2014; Rapacz-Kmita et al., 2015). Concerning topical use, montmorillonite has beneficial effects in dermatological and cosmetic applications (geotherapy, paleotherapy) (Carretero, 2002; López-Galindo et al., 2007).

The present work focuses on the assessment of a raw bentonite (Bt), a montmorillonite rich clay recently characterized in a previous work (Iannuccelli et al., 2016), for the development of a novel gentamicin/clay hybrid material for the topical use. Gentamicin (GM) is an aminoglycoside antibiotic widely used in the treatment of severe infections, caused by many Gram-negative and Gram-positive bacteria, such as meningitis, nephritis, and post-operative infections. Although it presents a very broad spectrum of action, its use is limited to serious infections caused by Gram-negative bacteria because of its high toxicity. Gentamicin is commonly administered as injections, topical and ophthalmic dosage forms because of poor absorption following the oral administration. The well-known poor gastrointestinal membrane permeability and the consequent low bioavailability (class III of the biopharmaceutical classification system) are likely connected to the high polarity of this cationic compound. Various approaches have been investigated in order to increase GM oral bioavailability, including the co-administration of absorption-enhancing agents such as surfactants (Hu et al., 2001; Ito et al., 2005), bile salts and glucosteroids (Axelrod et al., 1998), and liposaccharides (Ross et al., 2004). Although good gastrointestinal absorption enhancing effects were demonstrated, cytotoxicity and damage to the mucosa have been reported (Aungst, 2000; Ross et al., 2004; Swenson et al., 1994). Another strategy aiming to promote GM oral bioavailability could involve the use of microparticulate carriers to be taken up by the intestinal lymphoid tissue (des Rieux et al., 2007; Hussain et al., 2001; Iannuccelli et al., 2011; McClean et al., 1998; Moyes et al., 2007) or to be implanted for bone infection treatment also exploiting drug interaction with anionic polymers (Iannuccelli et al., 1996, 2011). Gentamicin is extensively used topically against severe microbial infections especially in burns and wounds (Chang et al., 2006), but also in the treatment of impetigo, infected bed sores, nasal staphylococcal carrier state, pyoderma, infections of the external eye, and adnexa (Nishijima and Kurokawa, 2002). Gentamicin applied to the skin has only a low systemic absorption due to the difficult penetration through the deep layers of the skin, related, probably, to its cationic nature; for this reason, its use is limited to the local effect that involves mainly the most superficial skin layers. Despite its benefits, GM short-life, bacterial

barriers and adverse effects such as nephrotoxicity, ototoxicity, and neurotoxicity upon prolonged use limit GM daily dosage (Roberts, 2007). In fact, many clinicians are reluctant to use it, even for a short term (Drusano, 2007). Efforts have been made to reduce toxicity associated with prolonged use by means of liposomes, micellar systems, hydrogels, microgels, or nanospheres (Ahangari et al., 2013; Ayhan and Ozkan, 2007; Changez et al., 2003; Eljarrat-Binstock et al., 2004; Jia et al., 2008; Nnamani et al., 2013; Sòkmen et al., 2008; Umeyor et al., 2012). Local delivery of GM can solve the major disadvantages of the systemic administration by maintaining a high local antibiotic concentration for an extended time (Zalavras et al., 2004). Particularly, drug delivery systems exhibiting high initial release rate followed by a sustained release at an effective antibiotic concentration may allow local control of infection while minimizing side effects and preventing bacterial resistance (Aviv et al., 2007; Persson et al., 2006).

The preparation of a GM-based organo-modified bentonite (Bt/GM) may therefore represent a valuable alternative to assure safer and more effective utilization of GM for topical treatment. Based on these premises, the present research includes a thorough characterization of Bt/GM by means of several instrumental analyses as well as the comparison of the experimental results with Molecular Dynamics simulations (MD modeling) to provide a more detailed understanding about the interlayer arrangement and interactions promoted by the organic guest molecules confined in the montmorillonite framework. Moreover, GM antimicrobial activity, *in vitro* desorption, and *in vivo* skin permeation on human beings were assessed in the perspective of contribution to a novel antibiotic material.

2. Experimental part

2.1. Materials

A bentonite (Bt) of volcanic origin from Iglesias (Sardinia, Italy) deposit (average mineralogical composition from the producer's datasheet: montmorillonite 80%, quartz 13%, illite-kaolinite 5%, plagioclase 2%) was donated by Eurit srl (Colorobbia Group, Sovigliana Vinci, Italy). Gentamicin sulfate (GM, Fig. 1), composed of gentamicin C1 ($C_{21}H_{43}N_5O_7 \cdot H_2SO_4$, <45%), gentamicin C1a ($C_{19}H_{39}N_5O_7 \cdot H_2SO_4$, <35%), and gentamicin C2 ($C_{20}H_{41}N_5O_7 \cdot H_2SO_4$, <25%), pKa = 12.55 in acidic condition; 10.18 in basic condition, was purchased by Polichimica (Bologna, Italy). All the chemicals and reagents were of analytical grade (Sigma-Aldrich, Milan, Italy).

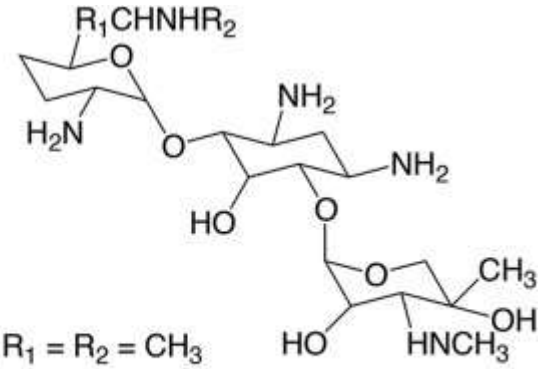

C1 (< 45%) $R_1 = R_2 = CH_3$
C2 (< 25%) $R_1 = CH_3$; $R_2 = H$
C1a (< 35%) $R_1 = R_2 = H$

Fig. 1. Molecular structure of gentamicin sulfate.

2.2. Bt activation

Bt activation and thus the implementation of its organophilic behavior are provided by the saturation of the montmorillonite interlayers with a homogeneous cationic population through the cation exchange reaction

hereafter detailed. A defined amount of Bt was grinded by a vibratory ball mill (Fritsch GmbH, Idar-Oberstein, Germany) for 10 h to remove particle aggregates. Batches of dispersions were prepared mixing 1 g of milled Bt and 25 mL of NaCl 0.1 M and were shaken with a magnetic stirrer at room temperature for 24 h. The supernatant was centrifuged (mod. 4235, 188 ALC International, Milan, Italy) at 2115 ×*g* for 20 min and the solid was twice subjected to the same treatment. The separated solids were washed several times with 35 mL of distilled water under magnetic stirring at room temperature for 4 h followed by centrifugation at 2115 ×*g* for 2 h. The solid was dried under vacuum at room temperature and the supernatant analyzed for NaCl absence by titration with 0.1 M silver nitrate solution according to U.S. Pharmacopeia. The activation process was carried out in triplicate.

2.3. Bt/GM preparation

Gentamicin was adsorbed onto both activated and non-activated Bt at constant drug concentration corresponding to about two times Bt CEC measured for activated Bt/GM (aBt/GM) and non-activated Bt/GM (Bt/GM), respectively. Glass tubes filled with 20 mL GM water solution (1 mg/mL) and 100 mg of milled Bt were horizontally shaken in the darkness for 24 h, a time suitable to fully saturate the montmorillonite interlayer with GM. The dispersions were centrifuged (2115 ×*g*, 20 min) and solids washed twice with 35 mL deionized water under magnetic stirring for 15 min. The obtained organo-modified clays were dried under vacuum at room temperature and stored in the darkness. Three batches were prepared for each sample.

2.4. Gentamicin adsorption measurements

In this paper, the term “adsorption” was used to generally refer to the immobilization of GM onto Bt thus without distinguish between intercalation in the interlayer of montmorillonite and adsorption on the outer surface of montmorillonite and illite-kaolinite. However, when dealing with each single mineral phase the term adsorption and intercalation will be suitably used.

The amount of GM adsorbed onto Bt in both aBt/GM and Bt/GM was calculated as the difference between the initial GM concentration and that in the supernatants obtained during organo-modified clay preparation. GM was derivatized by reaction with *o*-phtaldialdehyde of an aliquot of 1 mL from the supernatants according to Sampath and Robinson method (Sampath and Robinson, 1990) and determined spectrophotometrically (Lambda 3B, Perkin-Elmer, Norwalk, CT, USA) at 274 nm wavelength. The GM concentrations were expressed as drug/clay weight percentage as well as yield (actual/theoretical drug) percentage on three determinations from three different batches.

2.5. Size, surface charge, and pH value

Bt/GM particle size, Polydispersity Index (PDI), and *Z*-potential were determined on 10 mg/mL organo-modified clay water dispersion by using Photon Correlation Spectroscopy (PCS) (Zetasizer version 6.12, Malvern Instruments Ltd) equipped with a 4 mW He__Ne laser (633 nm) and a DTS software (Version 5.0) and compared with those of Bt. pH value of 2% Bt/GM water dispersion was measured by potentiometry immediately after the preparation of the dispersion and after 1 h; obtained data were compared with the value of Bt dispersion, according to U.S. Pharmacopeia monograph for bentonite, and with 0.1% (*w*/*v*) GM water solution. The reported values were averaged on three determinations from three different batches.

2.6. CHN elemental microanalysis

CHN elemental microanalysis (Elemental analyzer, mod. 1106, Carlo Erba, Milan, Italy) was performed on Bt/GM in comparison with bulk Bt and GM. The analysis was carried out in triplicate.

2.7. Elemental composition by EDX analysis

Clay elemental composition was determined by Energy Dispersive X-ray (EDX, Oxford INCA-350, FEI Company-Oxford Instruments, Oregon, USA) analysis coupled with an Environmental Scanning Electron Microscopy (ESEM, Quanta 200 Fei Company-Oxford Instruments). Elements can be identified qualitatively and semi-quantitatively in function of the X-ray energy emitted by their electrons transferring from a higher energy shell to a lower energy one. X-ray emission from Kα or Kβ levels of the atoms calcium, potassium, oxygen, sodium, magnesium, aluminum, silicon, and other elements with atomic numbers from 4 were recorded by the selected area method related to whole clay particles from samples mounted without a conductive coating on carbon stubs with the following experimental settings: low vacuum (0.70 Torr), accelerating voltage 12 kV, spot size 3, element detection limit ~0.05 wt%, spatial resolution 0.1 µm, total spectrum counts >250,000, accuracy within ±5% relative errors by reference to standards. EDX spectra representing the plots of X-ray counts (intensity) *vs.* energy peak (keV) of each element were acquired and semi-quantitative compositions, obtained by a standardless method of acquisition and expressed as relative weight percentage of each element, were calculated. The carbon peak at low energy level, related to the hydrocarbon contamination growing the carbon stub signal, was not considered (Rolland et al., 2004). The reported data were averaged on three determinations for each sample.

2.8. FT-IR measurements

FT-IR measurements were performed using a Perkin-Elmer FT-IR 1600 (abscissa accuracy of 0.01 cm^{-1} using HeNe laser reference; resolution from 2 to 16 cm^{-1}; lithium tantalite temperature-stabilized detector) on bulk GM, bulk Bt, Bt/GM, and Bt/GM physical mixture at GM content corresponding to that of the organo-modified clay. The samples were maintained in a drier, dispersed in a Nujol mull (typically 2% w/w) and measured. Spectra were collected in air in the MID Infra-Red (mid-IR) region. The analyses were performed in triplicate.

2.9. X-ray powder diffraction

X-ray powder diffraction (XRD) was employed mainly to detect basal periodicity variation in montmorillonite before and after treating Bt with GM. The XRD patterns were recorded from (00*l*) oriented mounts, in the temperature range from 25 to 500 °C with a heating rate of 10 °C/min using a PANalytical X'Pert PRO diffractometer equipped with X'Celerator detector. Before measurements all the samples were simultaneously equilibrated at the same environmental conditions. Experimental conditions were: Incident beam: monochromatic Cu $K\alpha_1$ radiation (1.54060 Å), 40 kV and 40 mA; filter, nickel; Soller slits, 0.04 rad; anti-scatter mask, 20 mm; anti-scatter slit, 1/4°; divergence slit, 1/4°. Diffracted beam: X-ray detector, X'Celerator (Position Sensitive Detector, PSD); anti-scatter mask, 5.0 mm; Soller slits, 0.04 rad; integration time, 20 s in continuous scanning (PSD length of 2.12°2θ corresponding to a step size of 0.0170°2θ). Diffraction patterns were recorded from 3 to 75° (2θ) at room temperature, and from 3 to 20° (2θ) when measuring in non-ambient temperature conditions. NIST corundum was used as calibrating standard.

2.10. Thermogravimetric measurements coupled with evolved gas mass spectrometry

Thermogravimetric analyses were performed with a Seiko SSC 5200 thermal analyzer equipped with a quadrupole mass spectrometer (ESS, GeneSys Quadstar 422) to analyze gases evolved during thermal reactions (MSEGA). This device samples gases *via* an inert, fused silicon capillary system, heated to prevent gas condensation. Analyses of evolved gas phases were carried out in multiple ion detection mode (MID), which allows the qualitative determination of evolved masses *vs.* temperature or time. MID analyses were carried out measuring the *m*/*z* ratios 17 and 18 for H_2O, 28 and 44 for CO_2, 30 for NO and NO_2, 34 for H_2S, 46 for NO_2, and 48, 64, 66 for SO_2, where m/z is the ratio between the mass number and the charge of an ion; SEM (Secondary Electron Multiplier) and FARADAY detectors operating at 900 V were employed with 1 s of integration time on each measured mass.

Measurements were performed on Bt, Bt/GM, and bulk GM air-dried samples at the following experimental conditions: heating rate: 10 °C/min for Bt and Bt/GM, and 20 °C/min for pure GM; heating range: 25–1000 °C (25–900 °C for pure GM); data measurement: every 0.5 s; purging gas: ultrapure helium, at a flow rate of 100 µL/min.

2.11. Differential scanning calorimetry

Bt/GM was subjected to thermal analysis on a Differential Scanning Calorimeter (DSC-4, Perkin-Elmer) and compared with GM and Bt/GM physical mixture at GM content corresponding to that of the organo-modified clay. The samples (6–7 mg) were accurately weighed in crimped aluminum pans and heated from 30 °C to 280 °C at a scanning rate of 10 °C/min under dry nitrogen flow (30 mL/min). All the thermograms were obtained in triplicate.

2.12. Molecular dynamics simulations

A $X_{0.75}[Si_{7.75}Al_{0.25}][Al_{3.5}Mg_{0.5}]O_{20}(OH)_4$ (X = monovalent cation) ideal montmorillonite model was used for the present study. This model shows −0.75*e* per unit cell, leading to a CEC of 101.9 meq/100 g, a value close to the experimental one. The simulation box consists of one layer made of 64 unit-cells corresponding to a basal surface of 4.14 nm × 7.17 nm. In order to mimic the partial cation exchange process obtained in the experiments, we consider the total negative charge of the layer to be counterbalanced by ~79.2% by C-1(GM) molecules and ~20.8% of sodium ions (see Supporting information for details). A certain amount of water molecules was also inserted in the interlayer (corresponding to the 2% wt.). In order to accommodate the organic cations, the interlayer distance was pre-expanded to 2.5 nm and the C-1 and water molecules and Na ions were randomly inserted. An initial energy minimization and MD simulation in the NPT-ensemble of 1 ns (298 K, 1 atm, time step 1 fs) have been used to optimize the interlayer region reaching an equilibrium density. Different initial starting configurations have been tested (in terms of organic, water, and sodium ions placement) and in all cases for a given system they converge to similar final arrangements and layer-to-layer distances. Then, the ones with the lowest energy have been further simulated for 1 ns in the NVT-ensemble. The last 0.5 ns have been used for the data analyses in terms of density profiles, pair correlation functions, ion coordinations. In all the simulations, both the atoms of the montmorillonite layer as well as the atoms confined in the interlayer were allowed to move and the periodic boundary conditions were applied. MD simulations were performed using the Discover module of the Materials Studio package (v. 5.0, Accelrys Inc.).

2.13. Antimicrobial activity

A microbiological agar well diffusion method was performed (Giamarellou et al., 1975) on Bt/GM in comparison with the respective physical mixture as well as pure GM and Bt. Tryptic soy agar (15 mL) and *Staphylococcus aureus* (*S. aureus*) strain ATCC 6538 or *Pseudomonas aeruginosa* (*P. aeruginosa*) strain ATCC 27853 (10^5 CFU/mL) were used as growth medium and indicator microorganisms, respectively. The wells in agar plates were filled with the samples in water dispersions (5 µg/mL, 100 µL). The glass plates were incubated at 37 °C overnight and zone inhibition diameters determined and related to GM concentration of standard water solutions. The analyses were made in triplicate.

2.14. *In vitro* gentamicin desorption

Gentamicin dissolution and desorption from the organo-modified clay were examined under sink conditions using the flow-through cell, USP Apparatus 4 (Dissotest CE-1, Sotax, Basil, Switzerland) on exactly weighed samples in 100 mL of phosphate buffer solutions (pH 5.4 or 7.4 according to the European Pharmacopeia) at a temperature of 37.0 ± 0.5 °C under a flow rate of 25 mL/min. The dissolved or desorbed concentration of drug was determined spectrophotometrically (Lambda 3B, Perkin-Elmer) following

derivatization according to Sampath and Robinson (Sampath and Robinson, 1990) at fixed time intervals for 3 h. The reported data were averaged on three determinations.

2.15. *In vivo* skin permeation

In vivo skin permeation study was carried out following the application of Bt/GM, Bt, and GM, mechanically mixed into petroleum jelly immediately before skin application, on both the two shaved volar forearms and forehead of 3 healthy Caucasian volunteers (2 females and 1 male, aged 20–62), free of any dermatological disorder after obtaining informed consent for the experimentation following the recommended guidelines as set out in the Declaration of Helsinki. A delineated area of 2 × 5 cm received 200 mg of each formulation containing pure GM (4 mg), Bt/GM (65 mg) both corresponding to GM dose of 0.4 mg/cm^2, or pure Bt (65 mg). The samples were homogeneously distributed by means of rubber gloves. After an application time of 60 min, which had been found to have a predictive value for penetration resulting from longer times of application (Howes et al., 1996), the *stratum corneum* (SC) was stripped twelve times by using an adhesive tape (Scotch Film Tape 600-3M). This number of stripped tapes is considered proper by Food and Drug Administration bioequivalence guidelines (Shah et al., 1998). The tapes were applied to the skin with a constant pressure by a 500 g roller. The first stripped tape was not considered in the penetration study because it represents unabsorbed materials. Twelve tapes stripped from SC that has received pure petrolatum jelly as well as from untreated SC were also assayed as controls. The tapes were combined into 2 groups (group 1: tapes 2–6; group 2: tapes 7–12) in order to increase determination sensitivity and subjected to an extraction procedure by isopropyl alcohol to determine GM according to the method described above. Data were expressed in penetrated GM percentage of the applied dose. A further tape-stripping test was conducted on the volunteers under the same conditions after a resting period of 14 days. Tapes n. 2, 6, and 12 were assayed by Energy Dispersive X-ray (EDX) analysis coupled with an Environmental Scanning Electron Microscopy (ESEM) using the selected area method. An area of 1.25 cm^2 of each tape was cut from the center of the tape, mounted without conductive coating on a carbon stub. X-ray emission from Kα and Kβ levels of the atoms carbon, oxygen, aluminum, silicon, and sulfur were registered under the experimental setting described above. EDX spectra representing the plots of X-ray counts *vs.* elements and semi-quantitative results expressed as relative weight percentage of the elements present in the specimen were obtained. The reported data were averaged on the results obtained from the volunteers.

2.16. Statistical analysis

Data obtained were evaluated from a statistical point of view using ANOVA one-way. Differences at *p*-values < .05 were considered significant.

3. Results and discussion

Adsorption of GM onto Bt is essentially driven by the CEC of the clay that is related to isomorphic substitution in octahedral and tetrahedral sheets of montmorillonite. To modulate drug bioavailability through interactions with bentonite (Bt), the cationic gentamicin (GM) was selected. Each of the three major components of GM complex (C1, C1a, C2) contains five basic amino functions exhibiting change in protonation state of the amino groups as function of pH. At the acidic pH value of Bt/GM preparation, GM molecules carry almost fully protonated charges (+5 and +4) (Lesniak et al., 2003) that are appropriate for efficacious cation exchange on montmorillonite. The Bt selected to develop Bt/GM organo-modified clay was previously characterized providing information on mineralogical and physico-chemical features (Iannuccelli et al., 2016). Gentamicin capacity to be intercalated in a commercial montmorillonite to be used as general drug carrier has been demonstrated by Rapacz-Kmita et al. (2015, 2017). In the present work, more extensive knowledge about the specific interactions between GM and Bt was supplied providing information on the arrangement of the guest molecule in the montmorillonite interlayer as well as the potentiality of a topical application.

3.1. Interlayer structure

The first step of the research was to verify the usefulness of Bt activation procedure. Clay activation did not offer advantages in terms of GM adsorption extent (aBt/GM = 4.49 ± 0.56%, yield% = 25.13 ± 0.62; Bt/GM = 7.16 ± 0.91%, yield% = 35.29 ± 0.51). Therefore, the study was performed only on the non-activated Bt/GM.

Bentonite treatment with GM generated an increase of clay average particle size ($p > .05$) (Table 1) though remaining in the size range considered proper for several dermatological and cosmetic purposes (Lein and Oussoren, 2015). Both Bt and Bt/GM exhibited negative surface charge with a greater magnitude in Bt compared to Bt/GM ($p < .05$) (Table 1). Bentonite net surface charge is mainly due to montmorillonite pH-independent permanent structural charges accounting for 90–95% of the total charges (Au and Leong, 2016; Pecini and Avena, 2013). Furthermore, montmorillonite is characterized by a surface charge due to the hydrolysis of Si—O and Al—OH bonds on the external surfaces of tetrahedral sheets as well as along the edges. Consequently, the lower Bt/GM *Z*-potential in absolute value is probably ascribable to GM interactions with the edges of clay particles and/or acidic pH medium of GM water solution (Delgado et al., 1986; Furukawa et al., 2009). Upon contact with water, Bt provided alkaline dispersions (pH of about 9, Table 1), in agreement with the values required by both U.S. and European Pharmacopeias. Alkalinity, that remained unchanged after 1 h, is generated by quick diffusion from the interlayer surfaces of exchangeable Na^+ ions retained by electrostatic attraction. Conversely, Bt/GM water dispersions exhibited pH values consistent with those of pure GM suggesting the occurred exchange process between montmorillonite interlayer cations and GM.

Table 1
Size, polydispersity index (PDI), surface charge, and pH values of Bt, GM, and Bt/GM. Mean values ± SD.

Sample	Z-average (μm) ± SD	PDI	Z-potential (mV) ± SD	pH value
GM	–	–	–	4.52 ± 0.05
Bt	3.64 ± 0.98	0.42 ± 0.15	−28.40 ± 0.98	9.43 ± 0.48 (time = 0) 9.30 ± 0.07 (time = 1 h)
Bt/GM	6.82 ± 0.75	0.62 ± 0.12	−17.60 ± 1.30	4.66 ± 0.13 (time = 0) 4.91 ± 0.10 (time = 1 h)

In order to define the arrangement of GM molecules within montmorillonite lattice and elucidate the interaction mechanism occurring in Bt/GM, a suite of analyses was performed.

Elemental CHN analysis carried out on Bt/GM showed a C/N ratio in nice agreement ($p < .05$) with that of GM alone (Table 2) and therefore evidenced that the drug was present in the organo-modified clay.

Table 2
CHN microanalysis and C/N ratios of Bt, GM, and Bt/GM. Mean values ± SD.

Sample	C%	H%	N%	C/N
Bt	–	0.90 ± 0.21	–	–
GM	51.80 ± 1.05	8.91 ± 0.52	15.12 ± 0.83	3.43 ± 0.11
Bt/GM	2.28 ± 0.20	1.26 ± 0.23	0.63 ± 0.005	3.62 ± 0.30

The occurrence of a possible exchange process between GM and the exchangeable cations of montmorillonite as a preliminary evidence of GM intercalation was provided by Energy Dispersive X-ray (EDX) analysis carried out on Bt/GM compared with Bt. The identification and relative quantification analysis (Table 3, see Fig. S1) showed the Si and Al elements of tetrahedral and octahedral sheets, respectively, as well as Mg due to Al partial isomorphic substitution. Isomorphous substitutions in the octahedral sheets create an excess of negative structural charge within the lattice that is balanced by inorganic cations (mainly Na^+ and Ca^{2+}). A significant ($p < .05$) less abundance of Ca^{2+} ions in Bt/GM compared with those of Bt suggests the almost complete substitution of Ca^{2+} ions by the cationic form of GM and, consequently, a possible drug arrangement within montmorillonite interlayers. The detection of a

minimal content of S in the mixture suggests, however, a non-negligible intercalation of GM without losing the sulfate group.

Table 3
EDX semi-quantitative analysis of the elements present in Bt and Bt/GM samples. All data are expressed as relative percentage of the elements > 0.5%. Mean values ± SD.

	Bt	Bt/GM
O	32.25 ± 3.24	59.48 ± 0.63
Na	1.13 ± 0.73	0.90 ± 0.25
Mg	0.79 ± 0.59	0.71 ± 0.20
Al	11.01 ± 0.76	7.32 ± 0.23
Si	46.92 ± 2.42	27.99 ± 0.45
S	–	0.26 ± 0.20
K	2.38 ± 0.60	1.47 ± 0.17
Ca	2.30 ± 0.59	0.44 ± 0.16
Fe	3.22 ± 0.86	1.43 ± 0.27

Nonetheless, it has to be considered that GM could interact also with additional negative polar sites at the broken edges as well as by exposed hydroxyl end-groups on the terminated planes.

Another preliminary evidence was provided by mid-IR spectroscopy (see Fig. S2). The most relevant feature of the mid-IR spectra is the band at about 3400 cm^{-1}, related to the overlapping of asymmetric v_3 and symmetric v_1(H—O—H) stretching vibrations of water bound by hydrogen bonds in the interlayer (Farmer, 1974). Unlike in Bt and Bt/GM physical mixture, the band position in the Bt/GM shift to a lower value, suggesting a decrease of the coordinated water amount induced by the substitution of the exchangeable cations of montmorillonite by GM. This conclusion is supported by the shift of the shoulder at about 3250 cm^{-1} related to the overtone ($2v_2$) of the bending mode of the solvated water (Farmer, 1974) and by the positions of the absorption bands at about 1635 cm^{-1} attributable to v_2 (H—O—H) bending vibration. The position of this band is the same in Bt and Bt/GM physical mixture (~1637 cm^{-1}), it is instead moved to a lower value (~1628 cm^{-1}) in the Bt/GM suggesting a decrease of the coordinated water amount as demonstrated also by Madejová et al. (2002) in samples where the amount of water has been decreased. Other features of the mid-IR spectra can be related both to montmorillonite and to other mineralogical phases as well (Iannuccelli et al., 2016). More in detail we refer to the bands at about (Madejová and Komadel, 2001): i) 3692 and 3620 cm^{-1} related to OH stretching of structural hydroxyl groups of kaolinite and montmorillonite, respectively; ii) 916 cm^{-1}, a band related to (AlAlOH) bending in montmorillonite; iii) 1100, 795 and 690 cm^{-1} related to the Si–O vibration of quartz; iv) 1030 cm^{-1} related to Si—O stretching vibration in montmorillonite. These features, however do not significantly change in Bt, Bt/GM and Bt/GM physical mixture suggesting that they are unaffected by the presence of the antibiotic.

The main technique for detecting structural variations such as changes in the basal periodicity of montmorillonite, is obtained by XRD. The comparison between XRD pattern of Bt and Bt/GM did not highlight considerable differences except for a minor reduction of d_{001} value in Bt/GM montmorillonite (d_{001} = 14.19 Å) respect to Bt montmorillonite (d_{001} = 14.95 Å). Hence, temperature controlled XRD analysis was performed to acquire more information about GM arrangement within montmorillonite framework. In fact, in montmorillonite the thickness of the interlayer depends greatly on the type of occupying molecules (e.g., cations, organic molecules, *etc.*) and on the amount of solvating water. Conversely, by measuring the variation of the distances between the stacked layers along the *c* axis (*i.e.*, the d values of the (00l) reflections) as a function of temperature, information can be acquired on the thermal stability of the molecules occupying the interlayer.

Fig. 2 compares the trends of d_{001} reflections of montmorillonite in Bt and Bt/GM samples. The most significant data of the comparison is the persistence of the periodicity of Bt/GM montmorillonite despite

the rapid decrease observed for Bt montmorillonite. In fact, at 150 °C Bt montmorillonite interlayer exhibited the typical value of the completely dehydrated interlayer (d_{001} = ~10 Å), and this value did not change until the occurring of framework collapse at about 600 °C. Conversely, the reduction of the interlayer spacing in Bt/GM montmorillonite only starts after 210 °C. Thermal analyses here after reported, in nice agreement with these finding, will better highlight that at about this temperature begins the thermal decomposition of the antibiotic.

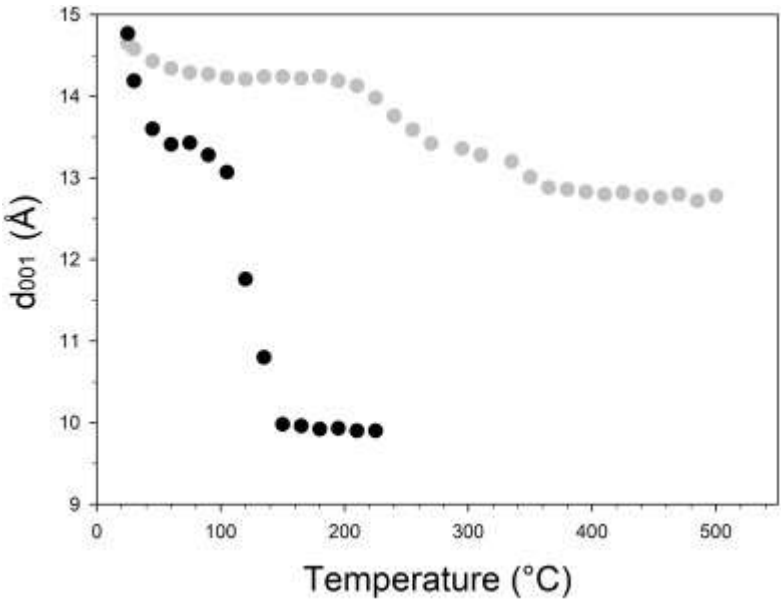

Fig. 2. Plot of d_{001} values for Bt (black circle) and Bt/GM (gray circle) montmorillonite as a function of temperature. The position of each (001) peak has been determined at the mid-height of the reflection, through the use of the software X-Pert High Score Plus. The error of the measurement falls within the dimensions of the used symbol.

Thermogravimetric (TG) and its first derivative (DTG) curves for GM are shown in Fig. 3. Five main reactions, with maxima at 80, 260, 317, 500, and 582 °C (DTG curve), lead to a nearly complete thermal decomposition of the antibiotic. The weight loss with maximum at 80 °C (mass loss of 14.7%, TG curve) is related to the removal of free water molecules, whereas reactions at higher temperature are related to the thermal decomposition of both the organic fraction and the sulfate group. The asymmetry and/or band-like shape of the DTG peaks, in particular for the thermal event that occurs at $T > 200$ °C, maybe related to the different forms (C1, C1a, and C2) of GM that thermally decomposed at significantly different temperature values.

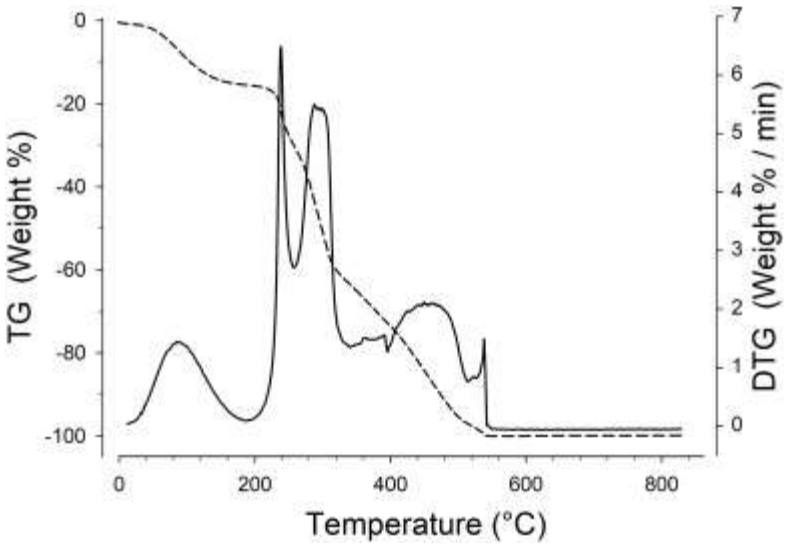

Fig. 3. TG (dashed line) and DTG curves (solid line) of GM.

The thermal behaviors of Bt and Bt/GM are compared in Fig. 4. The DTG curve (Fig. 4a) of Bt shows four thermal reactions with maxima at 103, 165, 485 and 645 °C. The first two reactions occurred between 25 and 210 °C and are attributed to the dehydration of montmorillonite with the removal of two water layers differently bound to the interlayer cation (maxima at 103 and 165 °C with mass losses of 9.0 and 0.84%, respectively - Fig. 4b). This finding is in agreement with the presence of divalent cations (Ca^{2+}) as major interlayer species (Iannuccelli et al., 2016; Mackenzie, 1970) and with XRD data (Fig. 2). The two reactions at higher temperature are ascribable to the dehydroxilation of the octahedral sheets of kaolinite (maximum at 485 °C, mass loss 1.2%) and montmorillonite (maximum at 645 °C, mass loss 1.9%). Differential thermal analyses (not reported) additionally evidenced an endothermic reaction with maximum at 573 °C related to the transition from the trigonal α to the hexagonal β form of quartz (Iannuccelli et al., 2016).

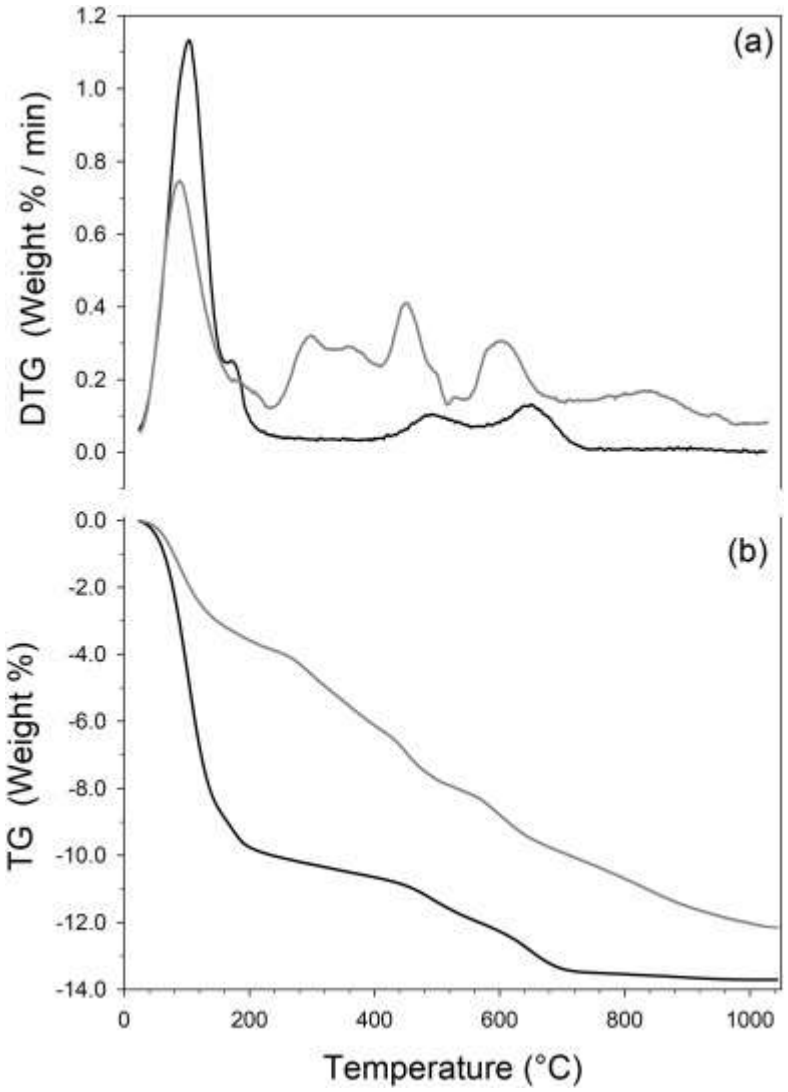

Fig. 4. DTG (a) and TG (b) curves of Bt (black line) and Bt/GM (gray line).

The TG and DTG curves of Bt/GM nearly parallel those of Bt, but with some major differences, arising from the presence of GM, that are: i) a drastic reduction of the mass loss related to the removal of hydration water (reactions between 25 and 235 °C, mass loss 3.85%); ii) two additional thermal events with maxima at 298 and 360 °C (reactions between 220 and 405 °C, mass loss 2.30%); iii) a shift toward lower temperature values of the two dehydroxilation reactions; iv) an additional thermal events with maximum at about 830 °C.

The lower amount of water in Bt/GM compared to Bt may explain the small difference in layer periodicity of montmorillonite measured by XRD at room temperature. The two reactions between 220 and 405 °C occur nearly in the same temperature of those observed for pure GM, however with a lower decomposition rate (DTG curve). As already pointed out, it is not negligible that the reaction at temperature at which starts the first of the two reactions (220 °C) is about the same at which begins the reduction of layer periodicity (Fig. 2). This finding may be thus definitively attributed to the beginning of the thermal decomposition of the intercalated antibiotic, as moreover suggested by MS-EGA curves.

The thermal decomposition of pure GM is complete at about 600 °C (Fig. 3); however, TG curves indicated that the intercalated antibiotic follows a different thermal path. More in detail, MS-EGA curves (see Fig. S3) indicated that the two just mentioned reactions lead to the release of H_2O (m/z = 18), NO (m/z = 30), and CO_2 (Fig. S3), further supporting the intercalation of GM. The detection of a MS-EGA signal for SO_2

highlights, however, the presence of marginal content of GM in its sulfate form, in accordance with the elemental analysis. XRD measurements showed that the layer periodicity of Bt/GM montmorillonite after the reaction with maximum at 360 °C was about 13 Å, higher than that in Bt montmorillonite (*i.e.*, 9.9 Å). It may be concluded that after the two thermal reactions occurring between 220 and 405 °C, a pillar-like residue, that thermally decomposes at higher temperature, forms in the interlayer of montmorillonite. However, as above mentioned, all these high temperature reactions (included the modification of the temperature at which occurred dehydroxilation) have not been taken into account in the present work, as they are related to the thermal evolution of the already decomposed antibiotic and mineral. Nevertheless, they well support the hypothesis of intercalation.

Further evidence supporting the intercalation of gentamicin is provided by DSC measurements that showed the absence of GM endothermic reaction in Bt/GM. On the opposite, this reaction is visible when DSC curves are collected for pure GM and physical mixture of Bt and GM.

Comparison of experimental measurements with MD simulations provided a more detailed understanding of the arrangement and bonding promoted by the GM molecules intercalated in montmorillonite. A computational approach attempted to simulate the interactions in the inter-structure of an ideal model of montmorillonite ($X_{0.75}[Si_{7.75}Al_{0.25}][Al_{3.5}Mg_{0.5}]O_{20}(OH)_4$ which corresponds to a CEC of 101.9 meq/100 g), gentamicin molecules (using C1 as a molecule model), sodium ions and solvent molecules (H_2O). Gentamicin components present both hydroxyl and amino groups and this affects the total positive charge (from 1 to 5 possible positive charge) of each molecule depending on the pH of the solution (Lesniak et al., 2003). In this study the system was simulated considering a pH ~ 5 aqueous environment corresponding to the preparation pH value at which GM molecules carry almost fully protonated charges (~85% of +5 and ~15% of +4), taking into account the distribution diagram of the different protonated species of component C1. This was achieved by inserting into the interlayer ~78.9% of molecules with +5 and ~21.1% molecules with 4+ charges and a certain content of water molecules (~2 wt%). Plus, in order to mimic the partial exchange process obtained experimentally a certain amount of sodium ions were also inserted. The simulated interlayer is made of ~79.2% of GM and ~20.8% of sodium ions with respect to the theoretical CEC. In this situation, the content of GM molecules useful to balance the negative charge of montmorillonite corresponds to an organic content of ~7.7% by weight.

Modeling results clearly show that Bt/GM is characterized by a monolayer arrangement of the GM (C1) molecules with a resulting layering periodicity of 14.2 ± 0.3 Å, a value in fair agreement with XRD finding (14.19 Å). The side and top views of a typical configuration of Bt/GM hybrid system optimized by simulation are shown in Fig. 5a and b. The analyses of density profiles show clear peaks for all the intercalated species. On the basis of radial distribution functions, the interatomic distance between the individual components of the sub-networks was further assessed. In particular, the ammonium H atoms of the GM molecules resulted located within the 2.1–2.9 Å range from the oxygen atoms of the montmorillonite surfaces, a distance slightly larger than those found in alkyl ammonium ions-based organoclays (1.8–2.5 Å) (Liu et al., 2007). This difference can be ascribed to the larger molecular flexibility of the alkyl ammonium cation due to its alkyl chain with respect to the more rigid and sterically hindered nature of the cyclic GM (C1) molecules. Both Na ions and the ammonium H atoms promote strong interactions with the oxygen atoms of the tetrahedral sheets (Fig. 5c and d), being mostly located above the surface siloxane rings (*i.e.* six-member rings). Water molecules partially affect such interactions by competing with the oxygen atoms of the tetrahedral sheets in promoting H-bonding with GM (C1) ammonium H atoms and hydroxyl groups and solvating the inner- and outer-sphere Na complexes (Brigatti et al., 2011).

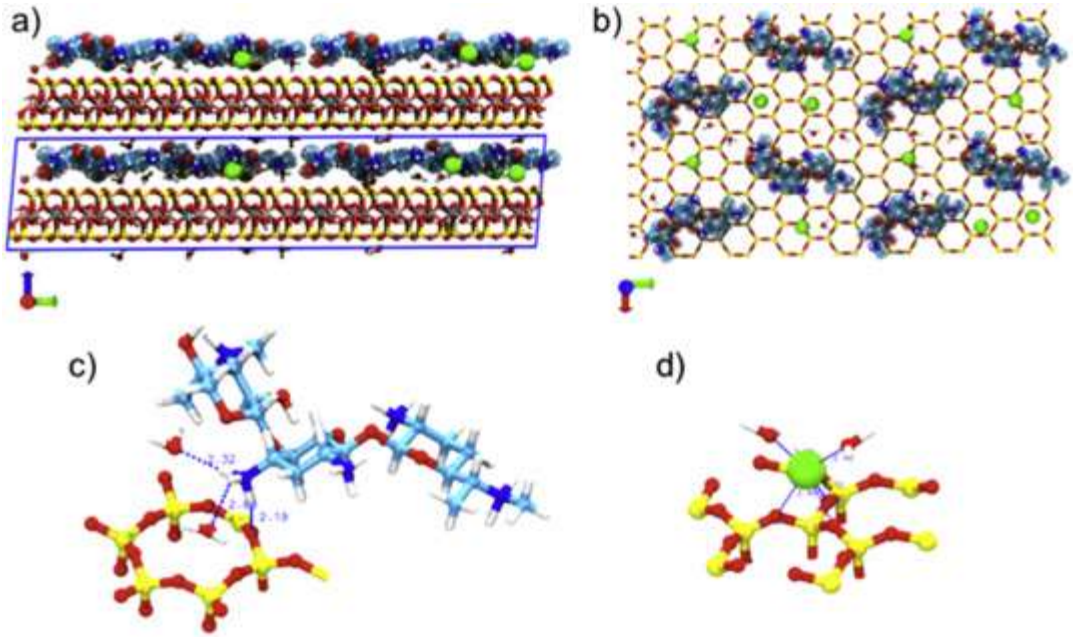

Fig. 5. a) Side view of montmorillonite in the Bt/GM hybrid system optimized by MD modeling. The simulated supercell is shown within the blue line and it is replicated twice along the z direction for clearness. b) Top view of the local arrangement of GM and water molecules and Na ions within the montmorillonite interlayer. c) Local environment around the GM ammonium group where the interaction between its hydrogen atoms with the oxygen of the tetrahedral sheets and the oxygen of water molecules are highlighted with a blue dashed line. d) Local coordination environment of a Na ion located on top of tetrahedral Al (Si substitution, charged site). For clearness, only the bottom siloxane sheet surface is shown. Color legend: Si atoms, yellow; O atoms, red; H atoms, white; C atoms, cyan; N atoms, blue; Na ions, green. (For interpretation of the references to color in this figure legend, the reader is referred to the web version of this article.)

3.2. Antibacterial activity and *in vivo* skin permeation

In a perspective of Bt/GM use as cutaneous drug delivery system for local or systemic control of infections, the study involved the evaluation of GM biological activity within the organo-modified Bt, *in vitro* desorption, and *in vivo* skin permeation on human beings. The biological activity of GM within Bt was assessed to point out a possible synergistic clay action. In fact, clay minerals, in particular smectites, have antimicrobial activity due to their high absorbing/adsorbing power with respect to water forming unfavorable hydrophobic conditions for the growth of microorganisms (Kim et al., 2016; Williams and Haydel, 2010). Antimicrobial activity of Bt/GM was determined on *S. aureus* or *P. aeruginosa* and compared with that of pure GM, pure Bt and the physical mixture of the antibiotic with the clay in the same ratio as Bt/GM.

The results obtained highlighted the absence of antimicrobial activity of the pure Bt and an almost complete activity of the physical mixture compared with pure GM (96.59 ± 5.68% against *S. aureus*, 88.01 ± 2.90% against *P. aeruginosa*). On the other hand, Bt/GM exhibited an activity against both the strains less than those obtained for GM solutions having the same antibiotic concentration (50.37 ± 1.59% against *S. aureus*, 50.07 ± 1.88% against *P. aeruginosa*). It is reasonable therefore to suppose that GM, though maintaining antibacterial activity against both Gram-positive and Gram-negative bacteria, desorbs from Bt/GM within the culture media of the agar plate incompletely indicating that drug intercalation between montmorillonite interlayer reduces drug availability (Ambrogi et al., 2017).

Nevertheless, complete GM desorption from Bt/GM was obtained at pH 5.5 buffer solution mimicking the acidic environment of skin surface (Fig. 6). Unlike the pure GM dissolving within 1 min regardless of the pH value, drug desorption profile involved a burst phase corresponding to about 40% of GM adsorbed onto Bt followed by a sustained phase reaching 100% drug delivered in about 2 h. Conversely, following a burst phase in which about 15% GM diffused into the medium, drug desorption at pH 7.4 was incomplete reaching a plateau corresponding to about 50% of GM payload after about 30 min. Burst phases could be related to GM fraction deposited or weakly linked to Bt particle surface whereas the subsequent phases to an exchange process between the intercalated GM and the cations present in the media reaching equilibrium according to the available cations (Joshi et al., 2009).

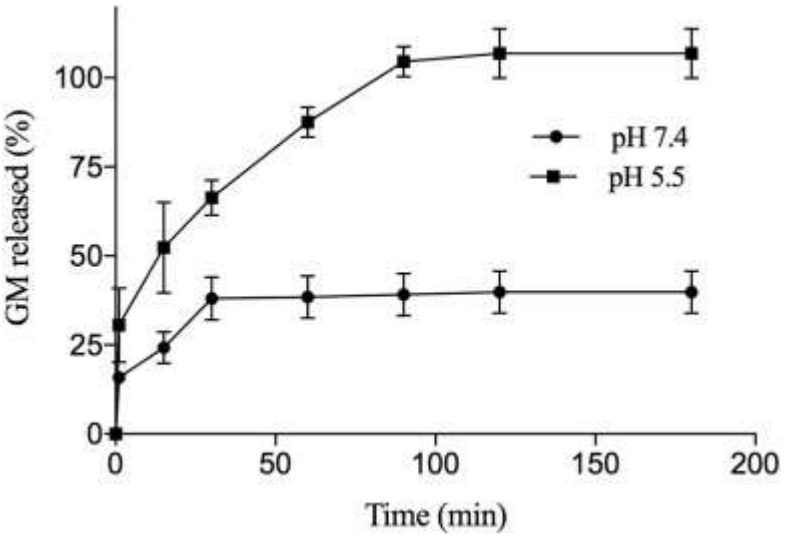

Fig. 6. Profiles of gentamicin desorption from Bt/GM in pH 5.5 and pH 7.4 media.

The higher GM percentage amounts desorbed at pH 5.5 with respect to pH 7.4 may reasonably arise from a competition by H^+ ions present in the assay medium on the same interaction sites of GM (Iannuccelli et al., 2015; Joshi et al., 2009). In biological fluids, physiological counter-ions can displace differently the drug from the substrate and deliver it into the body (Aguzzi et al., 2007).

The understanding of the mechanism by which insoluble particles can cross the *stratum corneum* (SC) is relevant to both prevent any possible local side effects or systemic exposure and properly exploit their potential benefits such as the reservoir role inside the hair follicles (Wosicka and Cal, 2010) or the drug transport modulation (Scalia et al., 2013). Since the passive transport through intact skin is considered highly unlikely (SCCP, 2007), particle penetration is most likely along the intercellular route following the lipid channels between the corneocytes and the appendage route along the hair follicles. Unlike the open question concerning nanoparticles, there is agreement that microparticles up to 10 µm can enter into the follicle orifices that can act as an efficient long-term drug reservoir (Lademann et al., 2007) from which soluble compounds could also diffuse into the viable epidermis (Borm et al., 2006). In relation to this, the density and size of hair follicles as well as the lipophilicity of the material applied on the skin have been assumed to contribute to differences in penetration rates (Feldmann and Maibach, 1967; Knorr et al., 2009; Otberg et al., 2004). To assess the mechanism by which the organo-modified bentonite enters the SC, the present study has considered the *in vivo* skin penetration profile of Bt/GM in comparison with that of pure GM and pure Bt applying the samples, incorporated in petroleum jelly, on human skin regions having two different hair follicle densities, the volar forearm (18 follicles/cm^2 corresponding to 0.09% skin surface, 78 µm diameter of hair follicle orifice) and the forehead (292 follicles/cm^2 corresponding to 1.28% skin surface, 66 µm diameter of hair follicle orifice) (Otberg et al., 2004).

The investigation was performed using EDX analysis on twelve repetitive stripped tapes containing the outermost layers of SC, generally the *stratum disjunctum* from the 2nd to the 5th tape, the *stratum compactum* from the 6th to the 12th tape (Jacobi et al., 2005) by both GM extraction from combined tapes and Bt detection on each tape. Skin exposure to pure GM at the level of the forehead region provided drug concentrations higher than those obtained on the volar forearm region ($p < .05$ concerning the first tape group) suggesting the involvement of the trans-follicular route pathway across SC. This assumption is consistent with the results from other Authors arguing that skin appendage route gained renewed interest for hydrophilic drugs representing a significant access also for gentamicin (Barry, 2002; Fadli et al., 2015; Ogiso et al., 2002). Moreover, GM levels are inclined to decrease with the increase of SC depth. The interaction of GM with Bt decreased antibiotic permeation extent compared with pure GM permeation ($p < .05$) leading to a constant GM concentration (about 2% of the applied dose), regardless of SC depth (Fig. 7).

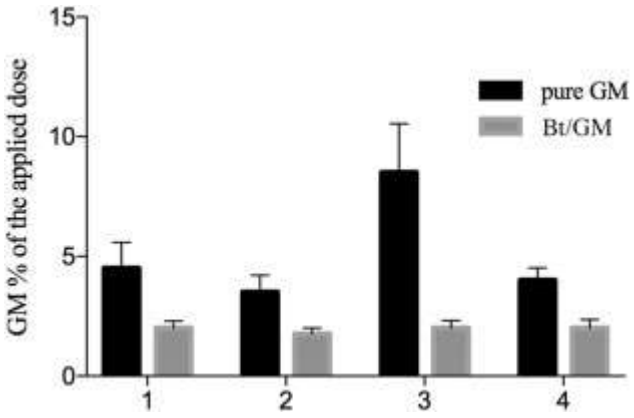

Fig. 7. GM permeated dose (% of the applied dose) across SC from pure GM and Bt/GM: (1) volar forearm, tape group 1 (tapes 2–6); (2) volar forearm, tape group 2 (tapes 7–12); (3) forehead, tape group 1 (tapes 2–6); (4) forehead, tape group 2 (tapes 7–12).

It follows a hampering effect of GM permeation provided by its reaction with Bt and the irrelevance of the application region, *i.e.* follicle density indicating presumably a different pathway. To monitor the possible translocation and distribution of Bt/GM across SC, each stripped tape (tapes 2, 6, and 12) was assayed by EDX analysis. All EDX spectra obtained from both pure Bt and Bt/GM skin exposure exhibited peaks from carbon, oxygen, aluminum, silicon, and sulfur atoms. The presence of sulfur in all tapes removed from untreated skin, attributable to the emission from SC keratin, prevented assessing the permeation of GM in its sulfate form. The elements Si and Al that are not naturally occurring elements in SC entail the presence of Bt (Cullander et al., 2000; Moretto et al., 1999). Accordingly, the presence of S atoms and the absence of Si and Al atoms were pointed out in all the control tapes (untreated skin and skin treated with only petroleum jelly). By measuring the intensity of characteristic X-rays spectra, the relative weight fraction of Si and Al can be calculated (Table 4).

Table 4
EDX analysis: relative element weight percentage detected on tapes 2, 6, and 12 following skin exposure to pure Bt and Bt/GM. Mean values ± SD.

	Volar forearm		Forehead	
Sample	Relative silicon weight	Relative aluminum weight	Relative silicon weight	Relative aluminum weight
pure Bt tape 2	29.3 ± 0.7	7.3 ± 0.3	13.7 ± 0.6	4.1 ± 0.5
pure Bt tape 6	3.9 ± 0.6	1.8 ± 0.6	5.5 ± 0.3	1.6 ± 0.3
pure Bt tape 12	5.3 ± 0.4	1.6 ± 0.4	5.3 ± 0.2	2.3 ± 0.2
Bt/GM tape 2	28.9 ± 0.4	7.0 ± 0.2	51.4 ± 0.9	10.8 ± 0.3
Bt/GM tape 6	17.6 ± 0.4	4.3 ± 0.3	18.0 ± 0.5	4.9 ± 0.3
Bt/GM tape 12	7.8 ± 0.5	2.4 ± 0.4	1.0 ± 0.5	1.6 ± 0.5

The detection of Si and Al atoms in all the tapes reveals the ability of clay particles to translocate across SC until the *stratum compactum* though Si and Al extents decreased with the increase of SC depth. Differences in quantitative distribution of Si and Al atoms between volar forearm and forehead application of both Bt and Bt/GM among the tapes were considered pointless to be argued. The limited influence of the sample exposure region is consistent with the results obtained by GM extraction from the tapes as the evidence of drug/clay association at the time of selecting SC pathway, plausibly different from the trans-follicular one. Besides skin appendages, SC is interrupted by inter-cluster corneocyte regions up to 100 µm in width, made of unsteady lipid packing generating openings having a low resistance to hydrophilic compounds (Cevc and Vierl, 2010; Dayan, 2005; Iannuccelli et al., 2013). Taking into account the size together with the hydrophilic nature of clayey samples, their motion along this trans-epidermal pathway could be considered as the favorite pathway. Moreover, Bt could increase SC hydration by means of the occlusive effect decreasing corneocyte packing and improving the clay transport. Such a route could also bypass the hindering effect on hydrophilic drug permeation provided by sebum along the trans-follicular route (Verma et al., 2016). Even if restricted to the superficial SC layers, it follows that a long-term Bt/GM reservoir for gradual GM release may be expected to perform leading to sustained antibacterial activity and minimized drug side effects.

4. Conclusions

The approach consisting of new carriers redeveloping already-approved drugs and excipients was addressed to modulate gentamicin release and skin permeation by exploiting drug arrangement in the interlayer of montmorillonite. Comprehensive examination of the organo-modified clay combined with a computational approach elucidated the mechanism of drug interaction with montmorillonite demonstrating the occurred intercalation. From that, gentamicin sustained desorption and the possible pathway across inter-cluster corneocyte regions of the *stratum corneum* may be ensued in the perspective of contribution to a novel antibiotic material offering a potential more effective anti-infective therapy.

Acknowledgements

The authors thank Prof. Gilberto Coppi from Department of Life Sciences, University of Modena and Reggio Emilia, for his expert and valuable support and Colorobbia Group, Porto Azzurro (Italy), for the kind gift of bentonite samples.

References

C. Aguzzi, C. Viseras, P. Cerezo, S. Rossi, F. Ferrari, A. López-Galindo, C. Caramella

Influence of dispersion conditions of two pharmaceutical grade clays on their interaction with some tetracyclines

Appl. Clay Sci., 30 (2005), pp. 79-86, 10.1016/j.clay.2005.03.007

C. Aguzzi, P. Cerezo, C. Viseras, C. Caramella

Use of clays as drug delivery systems: possibilities and limitations

Appl. Clay Sci., 36 (2007), pp. 22-36, 10.1016/j.clay.2006.06.015

A. Ahangari, M. Salouti, Z. Heidari, A.R. Kazemizadeh, A.A. Safari

Development of gentamicin-gold nanospheres for antimicrobial drug delivery to Staphylococcal infected foci

Drug Deliv., 20 (2013), pp. 34-39, 10.3109/10717544.2012.746402

581 V. Ambrogi, C. Carfagna, P. Cerruti, V. Marturano

582 **Additives in polymers**

583 C.F. Jasso-Gastinel, J.M. Kenny (Eds.), Modification of Polymer Properties, William Andrew Publishing
584 (2017), pp. 87-108, 10.1016/B978-0-323-44353-1.00004-X

585 P.-I. Au, Y.-K. Leong

586 **Surface chemistry and rheology of slurries of kaolinite and montmorillonite from different sources**

587 KONA Powder Part. J., 33 (2016), pp. 17-32, 10.14356/kona.2016007

588 B.J. Aungst

589 **Intestinal permeation enhancers**

590 J. Pharm. Sci., 89 (2000), pp. 429-442, 10.1002/(SICI)1520-6017(200004)89:4<429::AID-JPS1>3.0.CO;2-J

591 M. Aviv, I. Berdicevsky, M. Zilberman

592 **Gentamicin-loaded bioresorbable films for prevention of bacterial infections associated with orthopedic**
593 **implants**

594 J. Biomed. Mater. Res. A, 83A (2007), pp. 10-19, 10.1002/jbm.a.31184

595 H.R. Axelrod, J.S. Kim, C.B. Longley, E. Lipka, G.L. Amidon, R. Kakarla, Y.W. Hui, S.J. Weber, S. Choe, M.J.
596 Sofia

597 **Intestinal transport of gentamicin with a novel, glycosteroid drug transport agent**

598 Pharm. Res., 15 (1998), pp. 1876-1881

599 F. Ayhan, S. Ozkan

600 **Gentamicin release from photopolymerized PEG diacrylate and pHEMA hydrogel discs and their in vitro**
601 **antimicrobial activities**

602 Drug Deliv., 14 (2007), pp. 433-439, 10.1080/10717540701202911

603 B.W. Barry

604 **Drug delivery routes in skin: a novel approach**

605 Adv. Drug Deliv. Rev., 54 (Suppl. 1) (2002), pp. S31-40

606 M.L. Bello, A.M. Junior, B.A. Vieira, L.R.S. Dias, V.P. de Sousa, H.C. Castro, C.R. Rodrigues, L.M. Cabral

607 **Sodium montmorillonite/amine-containing drugs complexes: new insights on intercalated drugs**
608 **arrangement into layered carrier material**

609 PLoS One, 10 (2015), p. e0121110, 10.1371/journal.pone.0121110

610 T. Benelli, L. Mazzocchetti, E. D'Angelo, M. Lanzi, F. Saraga, L. Sambri, M.C. Franchini, L. Giorgini

611 **New nitrogen-rich heterocycles for organo-modified bentonites as flame retardant fillers in epoxy resin**
612 **nanocomposites**

613 Polym. Eng. Sci., 57 (2017), pp. 621-630, 10.1002/pen.24565

614 F.P. Bonina, M.L. Giannossi, L. Medici, C. Puglia, V. Summa, F. Tateo

615 **Adsorption of salicylic acid on bentonite and kaolin and release experiments**

616 Appl. Clay Sci, 36 (2007), pp. 77-85, 10.1016/j.clay.2006.07.008

617 P.J. Borm, D. Robbins, S. Haubold, T. Kuhlbusch, H. Fissan, K. Donaldson, R. Schins, V. Stone, W. Kreyling, J.
618 Lademann, J. Krutmann, D. Warheit, E. Oberdorster

619 **The potential risks of nanomaterials: a review carried out for ECETOC**

620 Part. Fibre Toxicol., 3 (2006), p. 11, 10.1186/1743-8977-3-11

621 M.F. Brigatti, E. Galan, B.K.G. Theng

622 **Structure and mineralogy of clay minerals**

623 F. Bergaya, B.K.G. Theng, G. Lagaly (Eds.), Handbook of Clay Science (2011), pp. 19-86

624 M.I. Carretero

625 **Clay minerals and their beneficial effects upon human health. A review**

626 Appl. Clay Sci., 21 (2002), pp. 155-163, 10.1016/S0169-1317(01)00085-0

627 G. Cevc, U. Vierl

628 **Nanotechnology and the transdermal route**

629 J. Control. Release, 141 (2010), pp. 277-299, 10.1016/j.jconrel.2009.10.016

630 H.-I. Chang, Y. Perrie, A.G.A. Coombes

631 **Delivery of the antibiotic gentamicin sulphate from precipitation cast matrices of polycaprolactone**

632 J. Control. Release, 110 (2006), pp. 414-421, 10.1016/j.jconrel.2005.10.028

633 M. Changez, K. Burugapalli, V. Koul, V. Choudhary

634 **The effect of composition of poly(acrylic acid)-gelatin hydrogel on gentamicin sulphate release: in vitro**

635 Biomaterials, 24 (2003), pp. 527-536

636 C. Cullander, S. Jeske, D. Imbert, P.G. Grant, G. Bench

637 **A quantitative minimally invasive assay for the detection of metals in the stratum corneum**

638 J. Pharm. Biomed. Anal., 22 (2000), pp. 265-279, 10.1016/S0731-7085(99)00248-4

639 N. Dayan

640 **Pathways for Skin Penetration. Cosmetics & Toiletries® magazine 120**

641 (2005), pp. 67-76

642 A. Delgado, F. González-Caballero, J.M. Bruque

643 **On the zeta potential and surface charge density of montmorillonite in aqueous electrolyte solutions**

644 J. Colloid Interface Sci., 113 (1986), pp. 203-211, 10.1016/0021-9797(86)90220-1

645 G.L. Drusano

646 **Pharmacokinetics and pharmacodynamics of antimicrobials**

Clin. Infect. Dis., 45 (Suppl. 1) (2007), pp. S89-95, 10.1086/518137

E. Eljarrat-Binstock, F. Raiskup, D. Stepensky, A.J. Domb, J. Frucht-Pery

Delivery of gentamicin to the rabbit eye by drug-loaded hydrogel iontophoresis

Invest. Ophthalmol. Vis. Sci., 45 (2004), pp. 2543-2548, 10.1167/iovs.03-1294

A. Fadli, K. Jiyauddin, S.J. Siti Nur, A.D. Samer, S. Budiasih, A. Jawad, M. Kaleemullah, S. Rasha, A.G. Mohammad Nizam, A. Ibrahim, H. Todo, K. Sugibayashi, Y. Eddy

Determination of permeation pathway of gentamicin into pig's ear skin

Int. Res. J. Pharm., 6 (2015), pp. 183-190

V.C. Farmer

The Infrared Spectra of Minerals

Mineralogical Society, Farmer, V.C., London, UK (1974)

R.J. Feldmann, H.I. Maibach

Regional variation in percutaneous penetration of 14C cortisol in man

J. Invest. Dermatol., 48 (1967), pp. 181-183

F. Forni, V. Iannuccelli, G. Coppi, M.A. Vandelli, R. Cameroni

Montmorillonite as a drug carrier: surface deposition of papaverine on the papaverine-veegum complex

Boll. Chim. Farm., 126 (1987), pp. 342-346

M.C. Franchini, P. Fabbri, A. Frache, G. Ori, M. Messori, C. Siligardi, A. Ricci

Bentonite-based organoclays as innovative flame retardants agents for SBS copolymer

J. Nanosci. Nanotechnol., 8 (2008), pp. 6316-6324

M.C. Franchini, M. Messori, G. Ori, C. Siligardi

Flame retardant SBS–clay nanocomposites

V. Mittal (Ed.), Thermally Stable and Flame Retardant Polymer Nanocomposites (2011), pp. 360-382

Y. Furukawa, J.L. Watkins, J. Kim, K.J. Curry, R.H. Bennett

Aggregation of montmorillonite and organic matter in aqueous media containing artificial seawater

Geochem. Trans., 10 (2009), p. 2, 10.1186/1467-4866-10-2

H. Giamarellou, V.M. Zimelis, D.O. Matulionis, G.G. Jackson

Assay of aminoglycoside antibiotics in clinical specimens

J. Infect. Dis., 132 (1975), pp. 399-406

D. Howes, R. Guy, J. Hadgraft, J. Heylings, U. Hoeck, F. Kemper, H. Maibach, J.P. Marty, H. Merk, J. Parra

Methods for Assessing Percutaneous Absorption: The Report and Recommendations of ECVAM Workshop 13

679 Altern. Lab. Anim. ATLA (1996)

680 Z. Hu, R. Tawa, T. Konishi, N. Shibata, K. Takada

681 **A novel emulsifier, labrasol, enhances gastrointestinal absorption of gentamicin**

682 Life Sci., 69 (2001), pp. 2899-2910

683 N. Hussain, V. Jaitley, A.T. Florence

684 **Recent advances in the understanding of uptake of microparticulates across the gastrointestinal**
685 **lymphatics**

686 Adv. Drug Deliv. Rev., 50 (2001), pp. 107-142

687 V. Iannuccelli, G. Coppi, R. Cameroni

688 **Biodegradable intraoperative system for bone infection treatment. I. The drug/polymer interaction**

689 Int. J. Pharm., 143 (1996), pp. 195-201, 10.1016/S0378-5173(96)04703-5

690 V. Iannuccelli, M. Montanari, D. Bertelli, F. Pellati, G. Coppi

691 **Microparticulate polyelectrolyte complexes for gentamicin transport across intestinal epithelia**

692 Drug Deliv., 18 (2011), pp. 26-37, 10.3109/10717544.2010.509362

693 V. Iannuccelli, G. Coppi, M. Romagnoli, S. Sergi, E. Leo

694 **In vivo detection of lipid-based nano- and microparticles in the outermost human stratum corneum by**
695 **EDX analysis**

696 Int. J. Pharm., 447 (2013), pp. 204-212, 10.1016/j.ijpharm.2013.03.002

697 V. Iannuccelli, E. Maretti, M. Montorsi, C. Rustichelli, F. Sacchetti, E. Leo

698 **Gastroretentive montmorillonite-tetracycline nanoclay for the treatment of *Helicobacter pylori* infection**

699 Int. J. Pharm., 493 (2015), pp. 295-304, 10.1016/j.ijpharm.2015.06.049

700 V. Iannuccelli, E. Maretti, F. Sacchetti, M. Romagnoli, A. Bellini, E. Truzzi, P. Miselli, E. Leo

701 **Characterization of natural clays from Italian deposits with focus on elemental composition and**
702 **exchange estimated by Edx analysis: potential pharmaceutical and cosmetic uses**

703 Clay Clay Miner., 64 (2016), pp. 719-731, 10.1346/CCMN.2016.064038

704 R.I. Iliescu, E. Andronescu, G. Voicu, A. Ficai, C.I. Covaliu

705 **Hybrid materials based on montmorillonite and citostatic drugs: preparation and characterization**

706 Appl. Clay Sci., 52 (2011), pp. 62-68, 10.1016/j.clay.2011.01.031

707 Y. Ito, T. Kusawake, M. Ishida, R. Tawa, N. Shibata, K. Takada

708 **Oral solid gentamicin preparation using emulsifier and adsorbent**

709 J. Control. Release, 105 (2005), pp. 23-31, 10.1016/j.jconrel.2005.03.017

710 U. Jacobi, H.-J. Weigmann, J. Ulrich, W. Sterry, J. Lademann

Estimation of the relative stratum corneum amount removed by tape stripping

Skin Res. Technol., 11 (2005), pp. 91-96, 10.1111/j.1600-0846.2005.00094.x

Y. Jia, H. Joly, A. Omri

Liposomes as a carrier for gentamicin delivery: development and evaluation of the physicochemical properties

Int. J. Pharm., 359 (2008), pp. 254-263, 10.1016/j.ijpharm.2008.03.035

G.V. Joshi, B.D. Kevadiya, H.A. Patel, H.C. Bajaj, R.V. Jasra

Montmorillonite as a drug delivery system: intercalation and in vitro release of timolol maleate

Int. J. Pharm., 374 (2009), pp. 53-57, 10.1016/j.ijpharm.2009.03.004

A. Kant, M. Datta

Organo montmorillonite as drug delivery vehicle for the extended release of an antibiotic drug

World J. Pharm. Res., 6 (2016), pp. 574-586

K.S. Katti, A.H. Ambre, N. Peterka, D.R. Katti

Use of unnatural amino acids for design of novel organomodified clays as components of nanocomposite biomaterials

Philos. Trans. A Math. Phys. Eng. Sci., 368 (2010), pp. 1963-1980, 10.1098/rsta.2010.0008

M.H. Kim, G. Choi, A. Elzatahry, A. Vinu, Y.B. Choy, J.-H. Choy

Review of clay-drug hybrid materials for biomedical applications: administration routes

Clay Clay Miner., 64 (2016), pp. 115-130, 10.1346/CCMN.2016.0640204

F. Knorr, J. Lademann, A. Patzelt, W. Sterry, U. Blume-Peytavi, A. Vogt

Follicular transport route – research progress and future perspectives

Eur. J. Pharm. Biopharm., 71 (2009), pp. 173-180, 10.1016/j.ejpb.2008.11.001

J. Lademann, H. Richter, A. Teichmann, N. Otberg, U. Blume-Peytavi, J. Luengo, B. Weiß, U.F. Schaefer, C.-M. Lehr, R. Wepf, W. Sterry

Nanoparticles – an efficient carrier for drug delivery into the hair follicles

Eur. J. Pharm. Biopharm., 66 (2007), pp. 159-164, 10.1016/j.ejpb.2006.10.019

A. Lein, C. Oussoren

Dermal

Practical Pharmaceutics, Springer, Cham (2015), pp. 229-263, 10.1007/978-3-319-15814-3_12

W. Lesniak, J. Mc Laren, W.R. Harris, V.L. Pecoraro, J. Schacht

An isocratic separation of underivatized gentamicin components, ^{1}H NMR assignment and protonation pattern

Carbohydr. Res., 338 (2003), pp. 2853-2862

744 X. Liu, X. Lu, R. Wang, H. Zhou, S. Xu

745 **Interlayer structure and dynamics of alkylammonium-intercalated Smectites with and without water: a**
746 **molecular dynamics study**

747 Clay Clay Miner., 55 (2007), pp. 554-564, 10.1346/CCMN.2007.0550602

748 A. López-Galindo, C. Viseras, P. Cerezo

749 **Compositional, technical and safety specifications of clays to be used as pharmaceutical and cosmetic**
750 **products**

751 Appl. Clay Sci., 36 (2007), pp. 51-63, 10.1016/j.clay.2006.06.016

752 R.C. Mackenzie

753 **Differential Thermal Analysis, Volume 1: Fundamental Aspects**

754 Academic Press, London (1970)

755 J. Madejová, P. Komadel

756 **Baseline studies of the clay minerals society source clays: infrared methods**

757 Clay Clay Miner., 49 (2001), pp. 410-432

758 J. Madejová, M. Janek, P. Komadel, H.-J. Herbert, H.C. Moog

759 **FTIR analyses of water in MX-80 bentonite compacted from high salinary salt solution systems**

760 Appl. Clay Sci., 20 (2002), pp. 255-271

761 S. McClean, E. Prosser, E. Meehan, D. O'Malley, N. Clarke, Z. Ramtoola, D. Brayden

762 **Binding and uptake of biodegradable poly-DL-lactide micro- and nanoparticles in intestinal epithelia**

763 Eur. J. Pharm. Sci., 6 (1998), pp. 153-163

764 W.S. Mohamed, A.B. Mostafa, H.E. Nasr

765 **Characterization and application of intercalated montmorillonite with verapamil and its polymethyl**
766 **methacrylate nanocomposite in drug delivery**

767 Polym.-Plast. Technol. Eng., 53 (2014), pp. 1425-1433, 10.1080/03602559.2014.909462

768 P. Moretto, J.E. Surleve-Bazeille, D. Licu, C. Michelet, P. Stoedzel

769 **Microanalysis of the human skin structure: preliminary results**

770 Nucl. Instrum. Methods Phys. Res. B, 158 (1999), pp. 386-392, 10.1016/S0168-583X(99)00346-8

771 A.B. Morgan, C.A. Wilkie

772 **Flame Retardant Polymer Nanocomposites**

773 John Wiley & Son, Hoboken, New Jersey, USA (2007)

774 S.M. Moyes, S.H. Smyth, A. Shipman, S. Long, J.F. Morris, K.E. Carr

775 **Parameters influencing intestinal epithelial permeability and microparticle uptake in vitro**

Int. J. Pharm., 337 (2007), pp. 133-141, 10.1016/j.ijpharm.2006.12.036

S. Nishijima, I. Kurokawa

Antimicrobial resistance of Staphylococcus aureus isolated from skin infections

Int. J. Antimicrob. Agents, 19 (2002), pp. 241-243

P.O. Nnamani, F.C. Kenechukwu, C.L. Anugwolu, A.C. Obumneme, A.A. Attama

Characterization and controlled release of gentamicin from novel hydrogels based on Poloxamer 407 and polyacrylic acids

Afr. J. Pharm. Pharmacol., 7 (2013), pp. 2540-2552

T. Ogiso, T. Shiraki, K. Okajima, T. Tanino, M. Iwaki, T. Wada

Transfollicular drug delivery: penetration of drugs through human scalp skin and comparison of penetration between scalp and abdominal skins in vitro

J. Drug Target., 10 (2002), pp. 369-378, 10.1080/1061186021000001814

N. Otberg, H. Richter, H. Schaefer, U. Blume-Peytavi, W. Sterry, J. Lademann

Variations of hair follicle size and distribution in different body sites

J. Invest. Dermatol., 122 (2004), pp. 14-19, 10.1046/j.0022-202X.2003.22110.x

L.B. de Paiva, A.R. Morales, F.R. Valenzuela Díaz

Organoclays: properties, preparation and applications

Appl. Clay Sci., 42 (2008), pp. 8-24, 10.1016/j.clay.2008.02.006

E.M. Pecini, M.J. Avena

Measuring the isoelectric point of the edges of clay mineral particles: the case of montmorillonite

Langmuir, 29 (2013), pp. 14926-14934, 10.1021/la403384g

G.R. Persson, G.E. Salvi, L.J.A. Heitz-Mayfield, N.P. Lang

Antimicrobial therapy using a local drug delivery system (Arestin) in the treatment of peri-implantitis. I: microbiological outcomes

Clin. Oral Implants Res., 17 (2006), pp. 386-393, 10.1111/j.1600-0501.2006.01269.x

A. Rapacz-Kmita, E. Stodolak-Zych, M. Ziabka, A. Rozycka, M. Dudek

Instrumental characterization of the smectite clay–gentamicin hybrids

Bull. Mater. Sci., 38 (2015), pp. 1069-1078, 10.1007/s12034-015-0943-7

A. Rapacz-Kmita, M.M. Bućko, E. Stodolak-Zych, M. Mikołajczyk, P. Dudek, M. Trybus

Characterisation, in vitro release study, and antibacterial activity of montmorillonite-gentamicin complex material

Mater Sci Eng C Mater Biol Appl, 70 (2017), pp. 471-478, 10.1016/j.msec.2016.09.031

A. des Rieux, V. Fievez, I. Théate, J. Mast, V. Préat, Y.-J. Schneider

An improved in vitro model of human intestinal follicle-associated epithelium to study nanoparticle transport by M cells

Eur. J. Pharm. Sci., 30 (2007), pp. 380-391, 10.1016/j.ejps.2006.12.006

M.S. Roberts

Dermal Absorption and Toxicity Assessment

(Second Edition), CRC Press (2007)

L.A. de S. Rodrigues, A. Figueiras, F. Veiga, R.M. de Freitas, L.C.C. Nunes, E.C. da Silva Filho, C.M. da Silva Leite

The systems containing clays and clay minerals from modified drug release: a review

Colloids Surf. B Biointerfaces, 103 (2013), pp. 642-651, 10.1016/j.colsurfb.2012.10.068

P. Rolland, V. Carlino, R. Vane

Improved carbon analysis with Evactron plasma cleaning

Microsc. Microanal., 10 (2004), pp. 964-965, 10.1017/S1431927604880504

B.P. Ross, S.E. DeCruz, T.B. Lynch, K. Davis-Goff, I. Toth

Design, synthesis, and evaluation of a liposaccharide drug delivery agent: application to the gastrointestinal absorption of gentamicin

J. Med. Chem., 47 (2004), pp. 1251-1258, 10.1021/jm030474j

S.S. Sampath, D.H. Robinson

Comparison of new and existing spectrophotometric methods for the analysis of tobramycin and other aminoglycosides

J. Pharm. Sci., 79 (1990), pp. 428-431

S. Scalia, E. Franceschinis, D. Bertelli, V. Iannuccelli

Comparative evaluation of the effect of permeation enhancers, lipid nanoparticles and colloidal silica on in vivo human skin penetration of quercetin

Skin Pharmacol. Physiol., 26 (2013), pp. 57-67, 10.1159/000345210

SCCP (Scientific Committee on Consumer Products)

Opinion on Safety of Nanomaterials in Cosmetic Products, SCCP/1147/07

European Commission (2007)

V.P. Shah, G.L. Flynn, A. Yacobi, H.I. Maibach, C. Bon, N.M. Fleischer, T.J. Franz, S.A. Kaplan, J. Kawamoto, L.J. Lesko, J.P. Marty, L.K. Pershing, H. Schaefer, J.A. Sequeira, S.P. Shrivastava, J. Wilkin, R.L. Williams

Bioequivalence of topical dermatological dosage forms—methods of evaluation of bioequivalence

Pharm. Res., 15 (1998), pp. 167-171

N. Sòkmen, F. Bican, F. Ayhan, H. Ayhan

Chelating agent effect on the release of gentamicin from PEG-DA hydrogels

Hacettepe J. Biol. Chem., 36 (2008), pp. 347-352

E.S. Swenson, W.B. Milisen, W. Curatolo

Intestinal permeability enhancement: efficacy, acute local toxicity, and reversibility

Pharm. Res., 11 (1994), pp. 1132-1142

E.C. Umeyor, F.C. Kenechukwu, J.D. Ogbonna, S.A. Chime, A. Attama

Preparation of novel solid lipid microparticles loaded with gentamicin and its evaluation in vitro and in vivo

J. Microencapsul., 29 (2012), pp. 296-307, 10.3109/02652048.2011.651495

A. Verma, A. Jain, P. Hurkat, S.K. Jain

Transfollicular drug delivery: current perspectives

Res. Rep. Transdermal Drug Deliv., 5 (2016), pp. 1-17, 10.2147/RRTD.S75809

L.B. Williams, S.E. Haydel

Evaluation of the medicinal use of clay minerals as antibacterial agents

Int. Geol. Rev., 52 (2010), pp. 745-770, 10.1080/00206811003679737

World Health Organization

Bentonite, kaolin, and selected clay minerals

Environmental Health Criteria 231, World Health Organization, Geneva (2005)

H. Wosicka, K. Cal

Targeting to the hair follicles: current status and potential

J. Dermatol. Sci., 57 (2010), pp. 83-89, 10.1016/j.jdermsci.2009.12.005

C.G. Zalavras, M.J. Patzakis, P. Holtom

Local antibiotic therapy in the treatment of open fractures and osteomyelitis

Clin. Orthop. (2004), pp. 86-93